Rapid Solution of Cosserat Rod Equations via a Nonlinear Partial Observer

2021 IEEE International Conference on Robotics and Automation. PREPRINT VERSION. ACCEPTED February 2020

Rapid Solution of Cosserat Rod Equations via a Nonlinear Partial Observer

Balint Thamo, Kev Dhaliwal, Mohsen Khadem

***Abstract*—The Cosserat rod equations are used to model continuum and soft robots. Solving these equations are computationally expensive, particularly due to mixed boundary values and kinematic constraints. In this paper, we present a novel nonlinear observer that can rapidly estimate the solution of the Cosserat rod equations. We present details of the observer design and analyse its convergence and stability. Furthermore, we compare the accuracy and performance of the observer with common solvers used in the literature. Our results show that the proposed observer can significantly improve the computational efficiency of continuum robots' models and estimates the solution of the Cosserat rod equations 7 times faster than common solvers.**

I. Introduction

Continuum and soft robots can traverse confined spaces and manipulate objects in complex environments. These robots benefit from mechanical compliance to offer safety and, simultaneously, approach the incredible capabilities of evolved living systems in complex tasks. Soft robots have been studied for variety of industrial applications [1]. Moreover, the enhanced dexterity and manipulability offered by continuum and soft robots enables increasingly less invasive and more complex procedures. They are envisioned as tools with significant potential impact in robotic surgery [2]. The most common approach for modeling of continuum and soft robots is using the Cosserat rod theory. Cosserat-based models have been developed and experimentally validated for tendon-driven robots [3], concentric tube robots [4], [5], multi-backbone robots [6], and fluidic actuated robots [7].

The Cosserat model estimates the continuum robots' backbone shape as a function of the robots mechanical characteristics and known external forces. It consists of several differential equations with boundary conditions split between the base and the tip of the rod. Thus, solving the model involves numerically solving a set of boundary value problems (BVPs), which can be computationally expensive. Several studies [8], [9] including our previous works [10], [11] have demonstrated implementation of fast enough solutions of Cosserat model for control of continuum robots. However, the computational cost of the model directly affects the performance and stability of these controllers. As a result less accurate models with low computational cost are still more attractive [12], [13].

Additionally, there are several promising new designs of continuum robots such as parallel concentric tube robots [6] and eccentric pre-curved tube robots [14] that consists of many kinematically coupled Cosserat rods. The computational cost of the Cosserat rod model is a significant obstacle in deployment of such designs and more efficient numerical methods are needed.

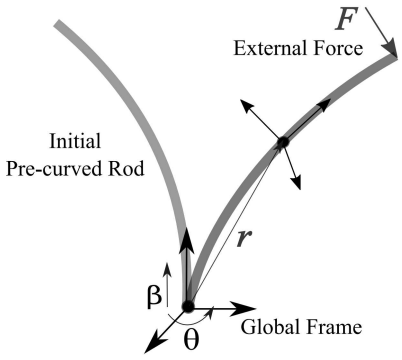

Fig. 1. A schematic of a Cosserat rod with and without external force. The actuation variables $\theta(t)$ and $\beta(t)$ denote the rotation, and translation of the rod's base, respectively.

Motivated by the above discussion, we study the design of a novel observer that can rapidly estimate the solution of Cosserat rod equations without the need to solve the BVP. The proposed observer employs partial measurement of a Cosserat rod's states (*i.e.*, curvatures at the end of the rod) to estimate the solution of the Cosserat equations. Furthermore, the convergence and stability of the observer is studied and it is shown that the observer predictions exponentially converge to the solution of the BVP. Simulations are performed to compare the performance of the observer with commonly used BVP solvers. Our algorithm is available online[1].

In Section II, the Cosserat rod equations are briefly reviewed. Section III outlines the detail of the observer design and study of the stability of the observer. In Section IV, simulations are performed to evaluate the performance of the observer in estimating the solution of the Cosserat equations. The results are compared with the existing BVP solvers in terms of accuracy and computational efficiency. Concluding remarks appear in Section V.

II. Review of Cosserat Rod Equations

Here, the Cosserat rod equations [5] are briefly reviewed. The following notation is used throughout the paper: x, $\boldsymbol{x}$, and $\mathbf{x}$ denote a scalar, a vector, and a matrix, respectively.

This research was supported by by the Medical Research Council [grants 8571708, and 8532390].

B. Thamo (corresponding author: b.thamo@sms.ed.ac.uk) and M. Khadem are with the School of Informatics, University of Edinburgh, UK. B. Thamo, M. Khadem and K. Dahliwal are with Translational Healthcare Technologies Group in the Centre for Inflammation Research, Queen's Medical Research Institute, Edinburgh, UK.

[1]https://github.com/SIRGLab/Rapid-Solution-of-Cosserat-Equations.git

A rod is modelled as a deformable curve with a frame attached to every point along its arclength, with the z-axis of the frame remaining tangent to the curve. A schematic of a rod under external forces is shown in Fig. 1. The configuration of the rod can be defined using a unique set of 3D centroids, $\boldsymbol{r}(s,t) : [0,\ell]\times[0,\infty] \rightarrow \mathbb{R}^3\times[0,\infty]$, and a family of orthogonal transformations, $\mathbf{R}(s,t) : [0,\ell]\times[0,\infty] \rightarrow SO(3)\times[0,\infty]$. Now, assuming the rod is made of linear elastic isotropic materials without pre-twist, we can derive the constitutive equations for calculating the instantaneous curvature of the rod $\boldsymbol{u}(s,t)$ and the overall shape of the rod.

$$\boldsymbol{r}^{'}(s,t) = \mathbf{R}(s,t)\boldsymbol{e}_3, \tag{1a}$$

$$\mathbf{R}^{'}(s,t) = \mathbf{R}(s,t)[\mathbf{u}(s,t)]_{\times}, \tag{1b}$$

$$\begin{aligned}\boldsymbol{u}^{'}(s,t) = -K^{-1}\Big[&[\mathbf{u}(s,t)]_{\times}K\big(\boldsymbol{u}(s,t)-\boldsymbol{u}^{*}\big)+\\ &[\boldsymbol{e}_3]_{\times}\mathbf{R}^{T}(s,t)\boldsymbol{F}(t)\Big]\end{aligned} \tag{1c}$$

where $^{'}$ denotes a derivative with respect to arc length s, the $[.]_{\times}$ operator is the isomorphism between a vector in $\mathbb{R}^3$ and its skew-symmetric cross product matrix, $\boldsymbol{e}_3 = [0,\ 0,\ 1]^T$ is the unit vector aligned with the z-axis of the global coordinate frame, $\boldsymbol{u}^*$ denotes the precurvature of the rod in its reference configuration, $\mathbf{K} = \text{diag}(EI, EI, GJ)$ is the stiffness matrix for the rod, E is the rod's Young's modulus, I is the second moment of inertia, G is the shear modulus, J is the polar moment of inertia, and $\boldsymbol{F}(t)$ denotes the external loads.

The boundary conditions for (1) are specified in terms of rod's initial curvatures, rotation $\theta(t)$, and translation $\beta(t)$ of the rod's base.

$$\boldsymbol{r}(0,t) = [0\ 0\ 0]^T, \tag{2a}$$

$$\mathbf{R}(0,t) = \mathbf{R}_z(\theta(t)), \tag{2b}$$

$$\boldsymbol{u}(\ell+\beta(t),t) = \boldsymbol{u}^*, \tag{2c}$$

where $\mathbf{R}_z$ denotes a rotation around the z axis and ℓ is the rod's initial length. The boundary conditions given in (2) define $\boldsymbol{r}$ and $\mathbf{R}$ at the base of the rod, and curvatures $\boldsymbol{u}$ at the end of the rod, thus forming a boundary value problem.

The model given in (1) is quasi-static. To solve the equations, it is assumed that at a given time, time-dependent variables are constant and the equations are solved in spatial domain (with respect to s). Shooting methods can be used to solve the boundary value problem. A shooting method consists of using a nonlinear root-finding algorithm to iteratively converge on values for $\boldsymbol{u}(0,t)$, in order to satisfy (2c). Next, the time-dependent variables are updated (*i.e.* $\theta(t)$, $\beta(t)$), and the equations are solved again in the spatial domain. Our main goal in this paper is to design an observer that will employ measurement of $\boldsymbol{u}(\ell+\beta(t),t)$ through time to estimate correct value of $\boldsymbol{u}(0,t)$ and ensure $\boldsymbol{u}(\ell+\beta(t),t) \rightarrow \boldsymbol{u}^*\ \forall t > 0$, without the need to solve the BVP iteratively.

III. Methodology

In this section, we design an observer that can rapidly estimate the rod's curvature $\boldsymbol{u}(s,t)$ in (1) without explicitly solving the boundary value problem. Our main assumption is that the solution of (1) is unique. We note that a Cosserat rod can buckle under external forces and exhibit elastic instabilities. In this case, solution of the Cosserat rod equations can oscillate between multiple equilibrium points. In practice, stability measures introduced in [15], [16] can be used to avoid the instabilities and ensure the solution of Cosserat equations remains unique.

A. Generalized Observable Cosserat Model

Here, we transform the Cosserat rod equations into an observable form that simplifies the design of the observer. To realize the effect of the missing initial value (*i.e.*, $\boldsymbol{u}(0,t)$) on the solution of the Cosserat equations, we define two auxiliary variables, namely,

$$\Gamma(s,t) := \frac{\partial \boldsymbol{u}(s,t)}{\partial \boldsymbol{u}(0,t)}, \tag{3a}$$

$$\chi(s,t) := \frac{\partial\big(\mathbf{R}^{T}(s,t)\boldsymbol{F}(t)\big)}{\partial \boldsymbol{u}(0,t)}. \tag{3b}$$

Using (3a) and the chain rule, the evolution of Cosserat rod's curvature in time can be estimated

$$\dot{\boldsymbol{u}}(s,t) = \Gamma(s,t)\dot{\boldsymbol{u}}(0,t). \tag{4}$$

We now use (1) to derive the equations for calculating $\Gamma(s,t)$ and $\chi(s,t)$. $\Gamma(s,t)$ can be computed by taking the partial derivative of (1c) with respect to $\boldsymbol{u}(0,t)$.

$$\begin{aligned}\Gamma^{'}(s,t) =&\mathbf{K}^{-1}\Big[[\mathbf{K}(\boldsymbol{u}(s,t)-\boldsymbol{u}^{*})]_{\times}\Gamma(s,t)-\\ &[\boldsymbol{u}(s,t)]_{\times}\mathbf{K}\Gamma(s,t)-[\boldsymbol{e}_3]_{\times}\chi(s,t)\Big].\end{aligned} \tag{5}$$

In deriving (5) we used the following identity

$$\frac{\partial([\boldsymbol{a}]_{\times}\boldsymbol{b})}{\partial \boldsymbol{c}} = -[\boldsymbol{b}]_{\times}\frac{\partial \boldsymbol{a}}{\partial \boldsymbol{c}} + [\boldsymbol{a}]_{\times}\frac{\partial \boldsymbol{b}}{\partial \boldsymbol{c}}. \tag{6}$$

We can calculate $\chi(s,t)$ in a similar way. First, we take the transpose of (1b). Next, we multiply both sides by $\boldsymbol{F}(t)$. Finally, taking partial derivative of both sides with respect to $\boldsymbol{u}(0,t)$ gives

$$\chi^{'}(s,t) = [\mathbf{R}^{T}(s,t)\boldsymbol{F}(t)]_{\times}\Gamma - [\boldsymbol{u}(s,t)]_{\times}\chi. \tag{7}$$

Remark 1. Based on our assumption on the uniqueness of the solution of the Cosserat rod equations, $\Gamma(s,t)$ defined in (3a) is a 3×3 matrix with rank of 3 if $\boldsymbol{u} \neq \vec{0}$. Moreover, based on (1) the initial values of $\Gamma(s,t)$ and $\chi(s,t)$ at $s = 0$ are $\mathbf{I}$ and $\mathbf{0}$, respectively. Also (5) and (7) are linear with respect to $\Gamma(s,t)$ and $\chi(s,t)$. Therefore, $\Gamma(s,t)$ and $\chi(s,t)$ are bounded for any bounded s. Considering that s is upper bounded by the length of the rod, both $\Gamma(s,t)$ and $\chi(s,t)$ are bounded for all t.

Now, using (1), (4), (5), and (7), we transform the Cosserat rod equations into an observable form.

$$\boldsymbol{r}^{'}(s,t) = \hat{\mathbf{R}}(s,t)\boldsymbol{e}_3, \tag{8a}$$

$$\mathbf{R}^{'}(s,t) = \hat{\mathbf{R}}(s,t)[\hat{\mathbf{u}}(s,t)]_{\times}, \tag{8b}$$

$$\chi^{'}(s,t) = [\mathbf{R}^{T}(s,t)\boldsymbol{F}(t)]_{\times}\Gamma - [\boldsymbol{u}(s,t)]_{\times}\chi, \tag{8c}$$

$$\begin{aligned}\Gamma^{'}(s,t) =&\mathbf{K}^{-1}\Big[[\mathbf{K}(\boldsymbol{u}(s,t)-\boldsymbol{u}^{*})]_{\times}\Gamma(s,t)- \\ &[\boldsymbol{u}(s,t)]_{\times}\mathbf{K}\Gamma(s,t) - [\boldsymbol{e}_3]_{\times}\chi(s,t)\Big],\end{aligned} \tag{8d}$$

$$\hat{\dot{\boldsymbol{u}}}(s,t) = \Gamma(s,t)\dot{\boldsymbol{u}}(0,t) \tag{8e}$$

with the following boundary conditions.

$$\boldsymbol{r}(0,t) = [0\ 0\ 0]^{T}, \tag{9a}$$

$$\mathbf{R}(0,t) = \mathbf{R}_z(\theta(t)), \tag{9b}$$

$$\Gamma(0,t) = \mathbf{I}, \tag{9c}$$

$$\chi(0,t) = \mathbf{0}, \tag{9d}$$

where $\hat{\boldsymbol{u}}(s,t)$ denotes the rod's curvature estimated by the observer.

B. Observer Design

Based on (2c), error of the observer in estimating the curvature of the rod at it's tip is

$$\boldsymbol{\epsilon}(t) = \hat{\boldsymbol{u}}(\ell+\beta(t),t) - \boldsymbol{u}^{*} \tag{10}$$

In the following theorem, we provide the solution for $\boldsymbol{u}(0,t)$ that drives the error in (10) to zero and ensures the solution of the observer in (8) converges to the solution of the boundary value problem in (1).

Theorem 1. With $\boldsymbol{u}(0,t)$ taken as

$$\boldsymbol{u}(0,t) = -\int_0^t \mathbf{R}\Gamma^{T}(\ell+\beta(t),t)\mathbf{P}\boldsymbol{\epsilon}(t)\mathrm{d}t, \tag{11}$$

where $\mathbf{P}(t)$ is the solution of the differential Riccati equation

$$\begin{aligned}-\dot{\mathbf{P}}(t) &= -\mathbf{P}(t)\Gamma^{T}(\ell+\beta(t),t)\mathbf{R}\Gamma(\ell+\beta(t),t)\mathbf{P}(t) + Q, \\ \mathbf{P}(t_f) &= \mathbf{P}_0,\end{aligned} \tag{12}$$

and $\mathbf{Q}$, $\mathbf{R}$, $\mathbf{P}_0$ are all symmetric positive definite matrices, the origin of (10) is exponentially stable and there exists positive constants c, k, and λ such that

$$\|\boldsymbol{\epsilon}(t_0)\| \leq c \Rightarrow \|\boldsymbol{\epsilon}(t)\| \leq ke^{-\lambda(t-t_0)}, \forall t \geq t_0 \geq 0 \tag{13}$$

Proof. Solution of the Riccati differential equation, $\mathbf{P}(t)$, is symmetric positive definite if $\Gamma^{T}(\ell+\beta(t),t)$ is bounded and non-singular [17]. Based on Remark 1 this condition is satisfied. Now, we select the following Lyapunov candidate

$$V = \boldsymbol{\epsilon}^{T}\mathbf{P}\boldsymbol{\epsilon}. \tag{14}$$

Taking the time derivative of V we obtain

$$\dot{V} = \dot{\boldsymbol{\epsilon}}^{T}\mathbf{P}\boldsymbol{\epsilon} + \boldsymbol{\epsilon}^{T}\dot{\mathbf{P}}\boldsymbol{\epsilon} + \boldsymbol{\epsilon}^{T}\mathbf{P}\dot{\boldsymbol{\epsilon}}. \tag{15}$$

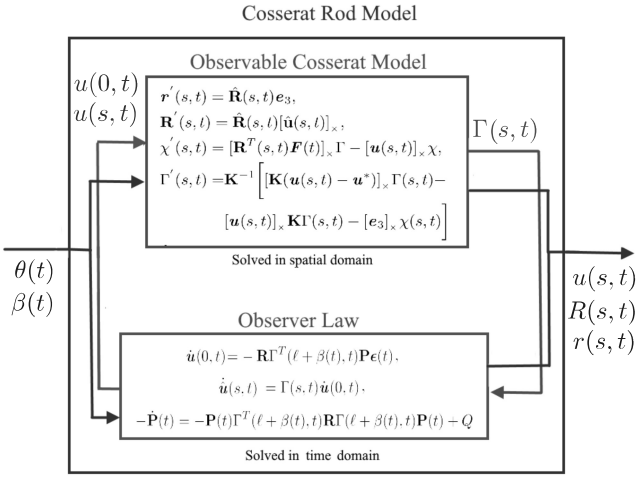

Fig. 2. A block diagram of the designed observer.

Additionally, from (10), (11), and (8e) we can calculate $\dot{\boldsymbol{\epsilon}}$ as

$$\dot{\boldsymbol{\epsilon}}(t) = \Gamma(\ell+\beta(t),t)\mathbf{R}\Gamma^{T}(\ell+\beta(t),t)\mathbf{P}\boldsymbol{\epsilon}(t). \tag{16}$$

Substituting (16) in (15) and sorting the equations gives

$$\begin{aligned}\dot{V} =&\boldsymbol{\epsilon}^{T}\Big(\dot{\mathbf{P}} - \mathbf{P}\Gamma^{T}(\ell+\beta(t),t)\mathbf{R}\Gamma(\ell+\beta(t),t)\mathbf{P} - \\ &\mathbf{P}\Gamma(\ell+\beta(t),t)\mathbf{R}\Gamma(\ell+\beta(t),t)^{T}\mathbf{P}\Big)\boldsymbol{\epsilon}\end{aligned} \tag{17}$$

Replacing $\dot{\mathbf{P}}$ using (12)

$$\dot{V} = \boldsymbol{\epsilon}^{T}\big(-\mathbf{Q} - \mathbf{P}\Gamma(\ell+\beta(t),t)\mathbf{R}\Gamma(\ell+\beta(t),t)^{T}\mathbf{P}\big)\boldsymbol{\epsilon} \tag{18}$$

$-\mathbf{Q}$ in (18) is uniformly negative definite in t by definition. $\mathbf{P}$ is symmetric, thus, $-\mathbf{P}\Gamma(\ell+\beta(t),t)\mathbf{R}\Gamma(\ell+\beta(t),t)^{T}\mathbf{P}$ has a quadratic form and is negative semi-definite uniformly in t. Hence their sum is negative definite uniformly in t. Thus, $\dot{V}$ satisfies the inequality

$$\dot{V} \leq -\alpha\|\epsilon\|. \tag{19}$$

Based on the Lyapunov Theorem and the foregoing inequality the origin of (10) is exponentially stable.

C. Implementation

The observer given in (8) is quasi-static, similar to the Cosserat equations in (1). However, it can be solved as an initial value problem using the initial values given in (9) and (11). At a given time t, time-dependent variables are assumed constant and the equations are solved in spatial domain using standard methods such as the Runge-Kutta or Adams–Bashforth families of algorithms. Next, the time-dependent variables are updated (*i.e.* $\boldsymbol{u}(0,t)$, $\mathbf{P}(t)$, $\theta(t)$, and $\beta(t)$). To calculate $\mathbf{P}(t)$, the Riccati differential equation in (12) should be solved backward in time from $t+t_f$, where t_f is desired finite time. The result should be stored in a memory. Next the updated time-dependant variables are used to solve the equations in the spatial domain again. This process is shown in Fig. 2.

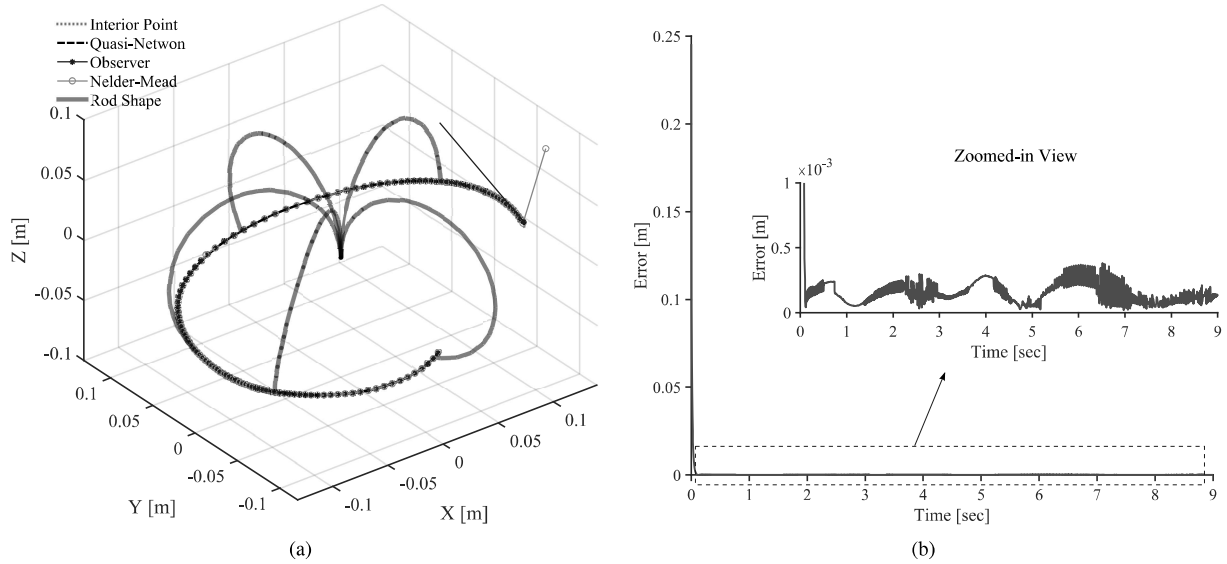

Fig. 3. (a) A comparison of rod's tip trajectory calculated by solving the rod's model using the observer and 3 different shooting methods. The rod's shape is shown at several configurations along the trajectory. (b) Error of the observer in estimating the position of the rod's tip with respect to the most accurate BVP solver, i.e., interior point method.

In the next section, we evaluate the performance of the observer in estimating the solution of Cosserat equations.

IV. Simulation Study

Simulations are performed to evaluate the proposed observer. Physical parameters of the rod used in the simulations are given in Table. I. The parameters are selected from the data-sheet of a rod made of Nitinol alloy with outer and inner diameters of 3 mm and 2 mm.

TABLE I
PHYSICAL PARAMETERS OF THE ROD.

ℓ [mm]	E [GPa]	G [GPa]
400	$70e9$	$10e9$
I [m^4]	J [m^4]	$\boldsymbol{u}^*$ [m^{-1}]
$3.1907e-12$	$6.3814e-12$	$[14,5,0]$

We compared the observer predictions with the solution of the rod equations computed using three different shooting methods. Each method employs a different root-finding algorithm, which to the best of authors knowledge, are the most commonly used BVP solvers. These solvers are:

1) Interior point method [18],
2) Quasi-Newton method with BFGS Hessian estimation [19],
3) Nelder-Mead method [20].

In the simulations, we rotated the rod at a frequency of $2\pi/10$ Hz and pushed the rod at a velocity of 10 mm/sec. Moreover, a time varying force equal to $[\sin(2\pi t/10),\ \cos(2\pi t/10),\ \sin(2\pi t/10)]^T$ was applied to the tip of the rod. The simulation runs for 10 seconds at sampling frequency of 200 Hz. The observer gains $\mathbf{R}$ and $\mathbf{Q}$ used in the simulations were set to $120\times\mathbf{I}$ and $30\times\mathbf{I}$, respectively. These values were found to achieve the minimum prediction error. The optimally tolerance for all the root-finding algorithms were set to 10^{-3}. Moreover, in all the shooting methods the estimated value of initial curvature at sample time k, i.e., $\boldsymbol{u}(0,t_k)$ was used as the initial guess for the root-finding algorithm in the next step $k+1$. This would make the shooting methods run faster. Moreover, in all the algorithms a 3(2) pair Runge-Kutta formula [21] was used to solve the differential equations governing the motion of the rod. The simulations are performed in Matlab on an Intel Core i7 (2.93 GHz) machine with 16 GB memory.

Fig. 3(a) shows the rod's trajectory estimated via the aforementioned BVP solvers and the observer. As it can be seen, accuracy of all of the methods are comparable. Also, it can be seen that the observer has an error at the first sampling time but rapidly converges to the correct solution. To investigate the accuracy of the observer, we compared the observer's predictions of the rod's tip position, $\boldsymbol{r}(\ell,t)$ with the results of the interior point method, which was found to be the most accurate BVP solver. The error measured as $\|\boldsymbol{r}(\ell,t)_{\text{observer}}-\boldsymbol{r}(\ell,t)_{\text{interior point}}\|$ is shown in Fig. 3(b). It can be seen that the observer rapidly converges to the final solution in less than 0.1 sec. After the convergence, the error of the observer remains below 0.4 mm with an average of 0.13 mm.

Fig. 4(a) shows the error of the solvers and the observer in satisfying the boundary conditions given in (2c). The error is measured as $\|\boldsymbol{u}(\ell,t)-\boldsymbol{u}^*\|$. The observer error is in the same order as the BVP solvers and remains below 0.06 m^{-1}. Fig. 4(b) compares the computational efficiency of the BVP solvers and the observer in terms of the time that each method takes to compute the solution of the model at each sampling time. The observer is much faster than the BVP solvers and has

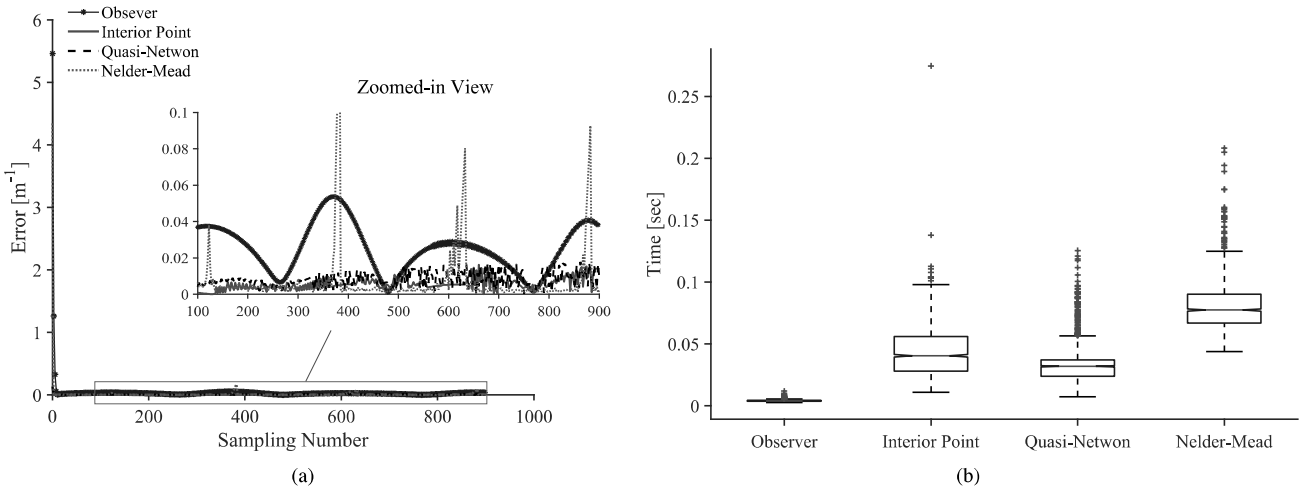

Fig. 4. (a) Accuracy of the observer in satisfying the boundary condition in (2c) compared with the BVP solvers. (b) A comparison of computational efficiency of the observer with common BVP solvers. On each box in (b), the central mark indicates the median, and the bottom and top edges of the box indicate the 25^{th} and 75^{th} percentiles, respectively. The whiskers extend to the most extreme data points and the outliers are plotted individually using plus symbol.

lower standard deviation. The average time that the observer takes to estimate the model's solution is 0.0042 seconds, which is significantly faster than other solvers. The fastest BVP method is Quasi-Newton method and can calculate the solution of the Cosserat equations in 0.0330 sec, which is more than 7 times slower.

TABLE II
EXPERIMENTAL RESULTS. MEAN ERROR (e_{MEAN}) MEASURED AS $\|\boldsymbol{u}(\ell,t)-\boldsymbol{u}^*\|$, STANDARD DEVIATION OF ERROR (σ_e), AVERAGE TIME TO ESTIMATE THE SOLUTION OF THE MODEL (t_{MEAN}) FOR EACH METHOD, AND STANDARD DEVIATION OF TIME σ_t ARE REPORTED.

	Observer	Interior-point	Quasi-Newton	Nelder-Mead
e_{mean} [m^{-1}]	0.0241	0.0055	0.0087	0.0101
σ_e [m^{-1}]	0.0537	0.0053	0.0065	0.1034
t_{mean} [sec]	0.0048	0.0525	0.0372	0.0810
σ_t [sec]	$7.4e-4$	0.021	0.0151	0.195

We performed 20 more simulations, where, rods with different dimensions were moved/rotated at frequencies varying between $\pi/5$ Hz and $\pi/50$. The results are summarized in Table II. The results demonstrate that the observer maintain similar error as the BVP solvers, while exhibiting superior computational efficiency. The mean error of the observer in satisfying the boundary conditions is 0.0241 m^{-1}. Considering the most accurate BVP solver, i.e, interior point method, as the ground truth, the observer has a mean error of 0.102 mm in predicting the rod's tip. This error is negligible and much lower than the experimentally validated accuracy of Cosserat equations, which is in the range of 3 to 10 mm [6]. The average time that the observer takes to estimate the model's solution is 7 times faster than the fastest BVP solver, namely, the Quasi-Newton method. The observer can estimate the solution of the Cosserat equations at sampling frequency of 200 HZ, while rendering similar accuracy to slower BVP solvers. The observer can significantly improve the computational efficiency of continuum and soft robots' models that include several kinematically coupled Cosserat rods.

V. CONCLUDING REMARKS

In this paper, we presented a new framework for solving the Cosserat rod equations. The Cosserat equations are widely used to model the motion of continuum and flexible robots. However, the computational cost of the model has impeded the widespread application of Cosserat-based models in real-time control of continuum robots. We have demonstrated that our numerical framework can estimate the model's solution 7 times faster than the fastest existing solvers, enabling future applications of Cosserat-based models in real-time control/motion-planning of continuum and soft robots.

REFERENCES

[1] F. Schmitt, O. Piccin, L. Barbé, and B. Bayle, "Soft robots manufacturing: A review," *Frontiers in Robotics and AI*, vol. 5, p. 84, 2018.

[2] J. Burgner-Kahrs, D. C. Rucker, and H. Choset, "Continuum robots for medical applications: A survey," *IEEE Trans. Robotics*, vol. 31, no. 6, pp. 1261–1280, Dec 2015.

[3] D. C. Rucker and R. J. Webster, "Statics and dynamics of continuum robots with general tendon routing and external loading," *IEEE Trans. Robotics*, vol. 27, no. 6, pp. 1033–1044, 2011.

[4] P. E. Dupont, J. Lock, B. Itkowitz, and E. Butler, "Design and control of concentric-tube robots," *IEEE Trans. Robotics*, vol. 26, no. 2, pp. 209–225, 2010.

[5] D. C. Rucker, B. A. Jones, and R. J. Webster, "A geometrically exact model for externally loaded concentric-tube continuum robots," *IEEE Trans. Robotics*, vol. 26, no. 5, pp. 769–780, 2010.

[6] C. B. Black, J. Till, and D. C. Rucker, "Parallel continuum robots: Modeling, analysis, and actuation-based force sensing," *IEEE Transactions on Robotics*, vol. 34, no. 1, pp. 29–47, 2018.

[7] F. Renda, M. Cianchetti, H. Abidi, J. Dias, and L. Seneviratne, "Screw-Based Modeling of Soft Manipulators With Tendon and Fluidic Actuation," *Journal of Mechanisms and Robotics*, vol. 9, no. 4, 05 2017.

[8] J. Till, C. E. Bryson, S. Chung, A. Orekhov, and D. C. Rucker, "Efficient computation of multiple coupled cosserat rod models for real-time simulation and control of parallel continuum manipulators," in *IEEE International Conference on Robotics and Automation (ICRA)*, 2015, pp. 5067–5074.

[9] R. Xu, A. Asadian, S. F. Atashzar, and R. V. Patel, "Real-time trajectory tracking for externally loaded concentric-tube robots," in *2014 IEEE International Conference on Robotics and Automation (ICRA)*, 2014, pp. 4374–4379.

[10] M. Khadem, J. O'Neill, Z. Mitros, L. da Cruz, and C. Bergeles, "Autonomous steering of concentric tube robots via nonlinear model predictive control," *IEEE Transactions on Robotics*, pp. 1–8, 2020.

[11] M. Khadem, J. O'Neill, Z. Mitros, L. d. Cruz, and C. Bergeles, "Autonomous steering of concentric tube robots for enhanced force/velocity manipulability," in *2019 IEEE/RSJ International Conference on Intelligent Robots and Systems (IROS)*, 2019, pp. 2197–2204.

[12] A. Bajo and N. Simaan, "Hybrid motion/force control of multi-backbone continuum robots," *The International Journal of Robotics Research*, vol. 35, no. 4, pp. 422–434, 2016.

[13] M. T. Chikhaoui, S. Lilge, S. Kleinschmidt, and J. Burgner-Kahrs, "Comparison of modeling approaches for a tendon actuated continuum robot with three extensible segments," *IEEE Robotics and Automation Letters*, vol. 4, no. 2, pp. 989–996, 2019.

[14] Z. Mitros, M. Khadem, C. Seneci, S. Ourselin, L. Da Cruz, and C. Bergeles, "Towards modelling multi-arm robots: Eccentric arrangement of concentric tubes," in *2018 7th IEEE International Conference on Biomedical Robotics and Biomechatronics (Biorob)*, 2018, pp. 43–48.

[15] H. B. Gilbert and *et al.*, "Elastic stability of concentric tube robots: A stability measure and design test," *IEEE Trans. Robotics*, vol. 32, no. 1, pp. 20–35, 2016.

[16] R. Xu, S. F. Atashzar, and R. V. Patel, "Kinematic instability in concentric-tube robots: Modeling and analysis," in *5th IEEE RAS/EMBS International Conference on Biomedical Robotics and Biomechatronics*, 2014, pp. 163–168.

[17] F. Callier and J. Willems, "Criterion for the convergence of the solution of the riccati differential equation," *IEEE Transactions on Automatic Control*, vol. 26, no. 6, pp. 1232–1242, 1981.

[18] J. Nocedal and S. Wright, *Interior-Point Methods for Nonlinear Programming*. New York, NY: Springer New York, 2006, pp. 563–597.

[19] F. E. Curtis and X. Que, "A quasi-Newton algorithm for nonconvex, nonsmooth optimization with global convergence guarantees," *Mathematical Programming Computation*, vol. 7, no. 4, pp. 399–428, 2015.

[20] M. J. D. Powell, "On search directions for minimization algorithms," *Mathematical Programming*, vol. 4, no. 1, pp. 193–201, 1973.

[21] P. Bogacki and L. Shampine, "A 3(2) pair of Runge - Kutta formulas," *Applied Mathematics Letters*, vol. 2, no. 4, pp. 321 – 325, 1989.